

## MD MODELING OF SCREW DISLOCATION - $\langle 100 \rangle$ LOOP INTERACTION IN Fe -

J. Marian and B. D. Wirth (*Lawrence Livermore National Laboratory*)

### Objective

The objective of this study is to develop improved atomistic insight into the mechanisms of dislocation interaction with radiation produced dislocation loops, which have a Burger's vector of  $a\langle 100 \rangle$ . This is required for the development of advanced constitutive relations for the mechanical behavior of irradiated steels and improved understanding of plastic flow localization.

### Summary

Ferritic/martensitic steels considered as candidate first-wall materials for fusion reactors experience significant radiation hardening at temperatures below  $\sim 400^\circ\text{C}$ . In this work we describe the motion of screw dislocations, known to control the plastic response of *bcc* materials to external stress, and their interaction with  $\langle 100 \rangle$  dislocation loops. MD simulations are used to simulate screw dislocation motion and, following a description of the computational method, we report the main physical mechanisms of the dislocation – loop interaction, including an estimate of the critical bowing angle and a first-order estimation of the induced hardening.

### Introduction

Ferritic steels and alloys represent a technologically important class of materials that are widely used for structural purposes in current nuclear fission reactors and proposed as candidate materials for plasma-facing first wall structures in future fusion energy facilities. Predicting their in-service performance requires understanding the accumulation of defects and evolution of the microstructure under the severe irradiation conditions found in these environments.

Hardening in the lower temperature regime is believed to arise from the formation of dislocation loops under irradiation that pin and may also decorate dislocations, thereby impeding their glide during deformation. A number of experimental studies performed over a wide range of temperatures in ferritic model alloys have shown the existence of large interstitial loops in the bulk, which may provide a significant contribution to the hardening caused during irradiation at lower temperatures [1]. The dislocation loops are observed with both  $\frac{1}{2} \langle 111 \rangle$  and  $\langle 100 \rangle$  Burgers vectors, although, generally, with a predominance of  $\langle 100 \rangle$  [2,3].

Ultimately, a high number density of dislocation loops in the appropriate temperature range can result in hardening by dislocation pinning, leading to a characteristic yield stress increase that can be measured experimentally using standard methods. In *b.c.c.* metals, screw dislocations dictate the plastic response and it is their behavior in the presence of irradiation-generated dislocation loops and the dynamics of their interactions that are key to understanding hardening in conditions relevant to fusion reactors. However, the atomistic nature of the interaction again makes these processes very difficult to study using conventional experimental techniques, whereas molecular dynamics (MD) has been successfully applied to a number of scenarios involving different lattice defects and dislocations [4,5]. In this report, we report the results of MD simulations of screw dislocation motion and interaction with a  $\langle 100 \rangle$  dislocation loop.

---

# Current address, Graduate Aeronautical Laboratories, California Institute of Technology, [jaimem@caltech.edu](mailto:jaimem@caltech.edu)

\* Current address, Nuclear Engineering Department, University of California, Berkeley, Berkeley, CA 94720-1730, [bdwirth@nuc.berkeley.edu](mailto:bdwirth@nuc.berkeley.edu)

The MD simulations presented in this paper have been carried out with the MDCASK code [6] using the Fe-Cu potentials developed by Ackland and co-workers [7].

## Results

### Estimation of the hardness due to $\{100\}$ loops

Based on Orowan's simple model, the most commonly used expression for the change in shear stress,  $\Delta\tau_s$ , induced in the dislocation glide plane by a regular array of defects is given in the following equation:

$$\Delta\tau_s = \alpha Gb(Nd)^{1/2} \quad (1)$$

where  $G$  is the shear modulus,  $b$  the Burgers vector of the dislocations,  $N$  the defect number density,  $d$  the defect diameter and the square-root factor is the reciprocal of the average distance between obstacles. The  $\alpha$  factor in equation (1) is known as the obstacle strength and is determined as  $\alpha = \cos(\phi/2)$ , where  $\phi$  is the angle in the line tension approximation at which the dislocation is able to break through the obstacle and continue its glide (for an impenetrable object  $\phi=0$ ,  $\alpha=1$ ). However, relatively few measurements of the critical angle have been made for radiation-induced defects and, in practice, microstructural observations and mechanical property measurements are compared to infer values of  $\alpha$  for different types of defects [8]. Atomistic simulations provide a direct calculation of the dislocation-obstacle interaction and critical bowing angle, which, together with other simulation methods, can provide all of the required input to equation (1). The computational elements necessary for this type of calculations are: (i) generation of a screw dislocation, (ii) introduction of an appropriate obstacle (*e.g.* a  $\{100\}$  loop), and (iii) the development of the capability to reproduce the conditions required for the interaction (*i.e.* temperature, stress, etc.). In what follows, we provide a self-consistent computational framework based on MD simulations to obtain an approximate value of  $\Delta\tau_s$ .

### Generation of a screw dislocation in $\alpha$ -Fe

The isotropic linear elasticity solution corrected with image summations for periodic boundary conditions is used to introduce a screw dislocation dipole into an otherwise perfect crystallite. In general, the introduction of a dipole, which is a measure intended for conserving the periodicity of the crystal, is not an appropriate initial condition for the simulations, as the dynamics of both dislocations are characterized by a strong self-annihilating bias. In order to remove one of the dislocation poles, the box must be cut accordingly, *i.e.* several atomic layers must be removed. This eliminates the periodicity in at least one direction, which further requires the use of appropriate boundary conditions. The computational

boxes employed in this study were  $100 \cdot a_0 \frac{\sqrt{3}}{2} \times 40 \cdot a_0 \sqrt{6} \times 50 \cdot a_0 \sqrt{2}$ , which amount to about  $10^6$

atoms. In general, for these large-scale simulations, flexible boundary conditions in the form of free surfaces have been used. These free surfaces have been generated in a way that is appropriate to the application of a desired shear stress in the computational box. After cutting the box to generate the free surfaces, the dislocation density is computed to be  $\rho = 2.9 \times 10^{15} \text{ m}^{-2}$ . Prior to any external application of stress, a relaxation of the linear-elastic dislocation configuration is performed at zero stress and a temperature-controlled equilibration at the target temperature. The stress (or more appropriately a surface traction) is applied on a skin region corresponding to the outermost atomic layers (one to three) adjacent to the free surfaces. The character and direction of the bounding surfaces and applied stress are considered concurrently to obtain the desired Peach-Köhler force (generally on  $\{110\}$  and  $\{112\}$  glide planes). In addition to this externally-induced force, image forces result from the existence of the traction-controlled (free) surfaces. These, together with the directional bias towards twinning orientations, are the sole forces exerted on the dislocation and upon which the dynamics of its motion are studied.

### Dislocation-obstacle interaction

The above knowledge of the dynamic constraints is required to appropriately position the obstacle in the presumed path of the dislocation. The obstacle was chosen to be a  $[100](100)$  dislocation loop with rhombic shape containing 113 interstitials ( $\sim 2$  nm).

A shear stress of 750 MPa was applied to the crystallite containing both the screw dislocation and the loop at a temperature of 100 K. Since the applied stress is below the computed Peierls stress (900 MPa for this potential), the dislocation begins to glide by a double-kink mechanism on  $\{110\}$  planes. Two out of the eight possible  $\{110\}$  planes become activated and the dislocation performs a serrated glide, generating kinks on both planes as well as on one  $\{112\}$  plane in the twinning sense, thus effectively moving on an “apparent” single  $\{112\}$  plane. In these simulations, the loop is also subject to the applied stress and undergoes several structural transformations prior to interacting with the dislocation. The whole process is illustrated in **Figure 1**. The loop’s corners initially transform into  $\frac{1}{2}[110]$  segments (**Figure 1 (a)**). In **Figure 1 (b)**, the right corner of the loop is subject to secession forces as the dislocation comes closer. This is a combination of multiple factors. First, the applied external and the dislocation stress fields superimpose to exert a force on the loop corners with  $\frac{1}{2}[110]$  geometry. Second, due to their prismatic nature, these  $\frac{1}{2}[110]$  segments are amenable to thermally activated diffusion along the direction of the dislocation line. Indeed, in **Figure 1 (c)** a perfect  $\frac{1}{2}[111]$  loop is emitted from the right section of the parent dislocation loop. At this point, the screw dislocation continues to move by a double-kink mechanism until it comes into contact with the central  $[100]$  section of the original loop. Finally, **Figure 1 (d)** shows the absorption of both the emitted loop (right side of the interaction) and the remaining  $\frac{1}{2}[110]$  corner situated at the left side. In both cases, heavily-arched, spiral segments of different dimensions are generated, leaving a central section consisting of a  $[100]$  loop and a pinned  $\frac{1}{2}[111]$  screw dislocation. In all cases, the Burgers vectors of the different screw dislocation and dislocation loop segments were determined by way of a 3D Burgers circuit analysis.

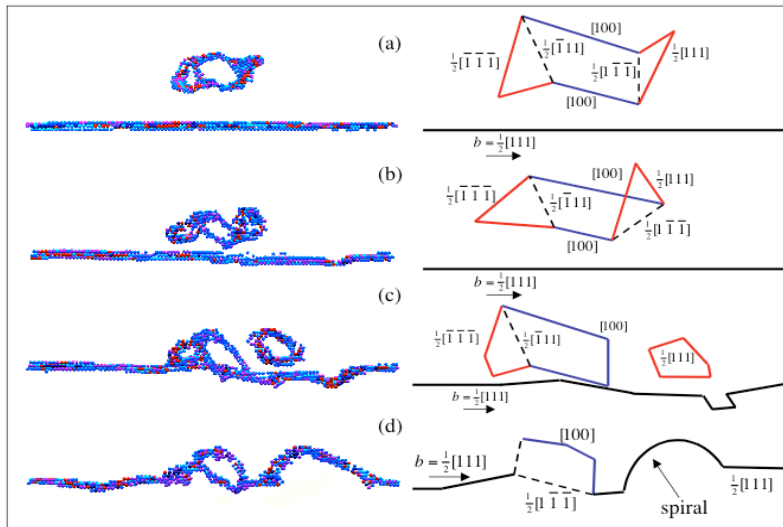


Figure 1 - Sequence of MD snapshots (left) and equivalent dislocation interpretation (right) of the interaction between a 113-SIA, rhombic  $[100]$  dislocation loop and a  $\frac{1}{2}[111]$  screw dislocation at 100 K and 750 MPa of applied shear stress. The dislocation and loop cores have been visualized using the centro-symmetry deviation parameter. Details of the interaction are given in the text.

The entire interaction process lasted for 150 ps (at strain rates of the order of  $\dot{\gamma} \approx 1.4 \times 10^8 \text{ s}^{-1}$ ) but, after 200 ps of annealing, the dislocation remained pinned and the only remarkable observation was the elastic transmission of the spiral (stretching) along the dislocation line. An increase in the applied shear stress was required to force the screw dislocation through the pinning obstacle.

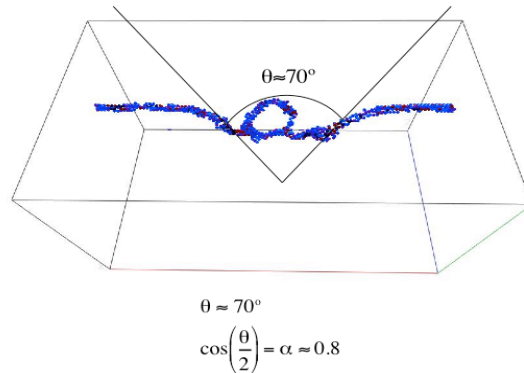


Figure 2 – Final snapshot before the dislocation breaks through the obstacle, leaving a [100] loop behind and two heavily-curved spirals along the dislocation line. The critical angle is  $\theta = 70^\circ$ , necessary to estimate the obstacle strength,  $\alpha = \cos(\theta/2) = 0.82$ .

#### Estimation of the hardening

The stress was gradually increased and applied to the pinned structure described above in 50 MPa increments. Only after a value of 1.0 GPa was the screw dislocation able to traverse the [100] loop. This increment in the external stress (250 MPa) is already a first-order estimate of the value of  $\Delta\tau_b$ . The dislocation starts to bow around the dislocation loop until, for  $\theta \approx 70^\circ$ , it can finally surpass the obstacle and continue with its normal unconstrained glide. **Figure 2** shows the last snapshot before the dislocation breaks free. From this value of  $\theta$ , one can calculate the obstacle strength,  $\alpha = \cos(\theta/2) = 0.82$ . With this and  $N = 1.2 \times 10^{23} \text{ m}^{-3}$ ,  $d = 2 \text{ nm}$  and  $K_a = 64 \text{ GPa}^1$ , one can compute the change in shear stress,  $\Delta\tau_b = 195 \text{ MPa}$ , due to equation (1). The computed value of  $\alpha$  suggests a higher obstacle strength for [100] loops than other calculations quoted in the literature [10,11]. Of course,  $N$  and  $d$  have been obtained directly from our computation box and are subject to the narrow applicability window of this MD simulation.  $N$  is unphysically high, with real values being two to three orders of magnitude lower. In addition, the product  $Nd$  inside the square root in equation (1) should in theory be an integral over the whole size spectrum. Further, it is not clear that the continuum line tension model used to calculate  $\alpha$  is applicable at the atomic dimension. Therefore, our results are only intended to provide a first-order estimate of  $\Delta\tau_b$ .

<sup>1</sup> Instead of  $G$ , it is more appropriate to use  $K_a$ .  $K_a$  is related to the anisotropic shear modulus and is obtained from the modified elastic compliances [9].

In uniaxial, tensile loading conditions, the resolved shear stress for polycrystalline materials that slip on {110} planes is related to the applied stress,  $\sigma_u$ , by [8]:

$$\tau_u = T\tau_s \quad (2),$$

where  $T$  is the Taylor factor and a standard value of 3.06 is commonly used for microstructure-mechanical property correlations [8]. Therefore, according to equation (2), we obtain  $\tau_u = 590$  MPa.

The calculations presented in this section suffer from obvious limitations. There is a strong statistical uncertainty associated with the single loop and interaction geometry considered, and to the conditions under which the simulations were performed. Also, the simulations have been carried out at strain rates that, although physically reasonable in some environments, are too high for the conditions expected in fusion steels. Our values of  $\tau$  and  $\tau_u$  are higher than those obtained experimentally or from other micromechanical estimations.  $\tau$ -values as high as 0.5 and 0.6 have been reported by Nicol *et al.* [10] and Hashimoto *et al.* [12], respectively, to describe yield stress changes of ~200 MPa and ~450 MPa, but our predicted values of 0.8 and 600 MPa are about 50% too large. As well,  $\tau$ -values in the range of 0.5 to 0.8 must be considered suspect based on the standard value of ~0.35 used to describe network dislocation reactions [13]. In any case, this work represents the first purely-dynamical study of dislocation-obstacle interactions involving  $\frac{1}{2}\langle 110 \rangle$  loops and screw dislocations in b.c.c. Fe and should be regarded as a first step in estimating the relevant hardening parameters by computer simulation. Recently, similar works involving edge and screw dislocations interacting with stacking fault tetrahedral, voids and precipitates have been reported [4,5,14], and it is expected that the knowledge of dislocation-obstacle interactions will significantly increase as new techniques and potentials are being developed.

## Conclusions

To study the elementary hardening process in irradiated  $\alpha$ -Fe, we have simulated the interaction between  $\frac{1}{2}\langle 110 \rangle$  screw dislocations and a large  $\frac{1}{2}\langle 100 \rangle$  loop. At 750 MPa of applied stress and 100 K, the interaction results in a complex combination of dislocation loop segment absorption and pinning. The dislocation's structure becomes significantly altered, with large spiral segments being the dominant feature. When the stress is increased to 1.0 GPa, the dislocation releases from the  $\frac{1}{2}\langle 100 \rangle$  loop at a critical angle of about 70°. These simulations permit calculation of the relevant parameters to estimate the hardening from Orowan's theory, most notably the obstacle strength of  $\tau = 0.82$ . Our results overestimate experimental results by approximately a factor of two, which may be attributed to the limited scope in terms of time and space scales available to MD simulations or possibly the limited applicability of the continuum line tension model at the atomic level. Future work will further investigate the spectrum of dislocation – obstacle interactions and investigate the appropriate connection between the atomic mechanisms and continuum hardening relationships.

## Acknowledgments

The authors are grateful to Drs. W. Cai and V. V. Bulatov for their help with the implementation of MD simulations of screw dislocation mobility. Useful discussions with Drs. A. Caro, M. Victoria and P. Derlet are acknowledged. This work has been performed under the auspices of the U.S. Department of Energy and Lawrence Livermore National Laboratory under contract W-7405-Eng-48 and within the CSN-UNESA Coordinated Research Programme under contract P000531499.

**References**

1. D. S. Gelles, M. L. Hamilton and R. Schäublin, in *Effects of Radiation on Materials: 20<sup>th</sup> International Symposium, ASTM STP 1405*, S. T. Rosinski, M. L. Grossbeck, T. R. Allen and A. S. Kumar, Eds., American Society for Testing and Materials, West Conshohocken, PA, 2002.
2. A. E. Ward and S. B. Fisher, *J. Nucl. Mat* **166** (1989) 227.
3. K. Suganuma and H. Kayano, *Radiat. Effects* **54** (1981) 81.
4. T. Harry and D. J. Bacon, *Acta Mater.* **50** (2002) 195; *Acta Mater.* **50** (2002) 209.
5. B.D. Wirth, V.V. Bulatov and T. Diaz de la Rubia, *Journal of Engineering Materials and Technology* **124** (2002) 329.
6. T. Diaz de la Rubia and M. W. Guinan, *Mater. Res. Forum* **174**, (1990) 151.
7. G. J. Ackland, D. J. Bacon, A. F. Calder and T. Harry, *Phil. Mag. A* **75**, (1998) 713.
8. R. E. Stoller and S. J. Zinkle, *J. Nucl. Mater.* **283-287** (2000) 349.
9. J. P. Hirth and J. Lothe, *Theory of Dislocations*, 2<sup>nd</sup> ed., Krieger Publishing Co. (1982) p. 168.
10. A.C. Nicol, M.L. Jenkins and M.A. Kirk, *Mat. Res. Soc. Symp.* **650** (2001) R1.3.
11. T. Takeyama, S. Ohnuki and H. Takahashi, *Trans. Iron and Steel Inst. Japan* **21** (1981) 326.
12. N. Hashimoto, S.J. Zinkle, R.L. Klueh, A.F. Rowcliffe, and K. Shiba, *Materials Research Society Symposium Proceedings Volume 650* (2001) R1.10.1.
13. P. Spatig, R. Schaublin and M. Victoria, *Materials Research Society Symposium Proceedings Volume 683E* (2001) BB1.10.1.
14. J. Marian, Ph. D. Thesis, Universidad Politécnica de Madrid (2002).